Available online at www.sciencedirect.com
ScienceDirect
Cement and Concrete Research 37 (2007) 691 – 702
Cement and Concrete Research

Effect of shrinkage-reducing admixtures on the properties of alkali-activated slag mortars and pastes

M. Palacios *, F. Puertas

Eduardo Torroja Institute Madrid, P.O. Box 19002, 28033 Madrid, Spain

Received 5 April 2005; accepted 8 November 2006

Abstract

The effect of a shrinkage-reducing admixture (SRA) based on polypropylenglycol on the dimensional stability of waterglass-activated slag mortars was studied. The analysis also showed the effect of the admixture on pore structure of the mortars as well as on the mineralogical composition and microstructure of the alkali-activated slag pastes.

The SRA reduced the shrinkage by up to 85 and 50% when the alkali-activated slag mortar specimens were cured at relative humidities of 99 and 50%, respectively. The mechanism primarily involved in shrinkage reduction is the decrease in the surface tension of pore water prompted by the admixture. The SRA also modified the pore structure – under both curing conditions – increasing the percentage of pores with diameters ranging from 1.0 to 0.1 μm. Capillary stress is much lower in these pores than in the smaller capillaries prevailing in mortars prepared without admixtures.

Microstructurally, the SRA occasioned a slight increase in the proportion of Si units Q^2 in the CSH gel and a decrease in the percentage of Al replacing the Si in the gel structure. The admixture did not, however, modify the mineralogical composition of the pastes.

Finally, the SRA admixture retarded the alkaline activation of the slag, more intensely at higher admixture dosages. While the admixture did not significantly alter the degree of reaction in pastes cured for 7 days at RH = 99%, the value of this parameter dropped by 7% in the presence of the admixture in pastes cured at 50% relative humidity.
© 2007 Elsevier Ltd. All rights reserved.

Keywords: Alkali activated slag; Granulated blast-furnace slag; Shrinkage; Admixture

1. Introduction

Alkali-activated slag (AAS) binders have taken a great interest from researches due to its manufacturing process which has important benefits from the point of view of the lower energy requirements and lower emission of greenhouses gases with respect to the manufacturing of Portland cement. Several studies [1–4] indicate that AAS cements and concretes present high mechanical strength and good performance in chemical attack, frost-thaw cycles and high temperatures. The main applications of these binders is in pre-casting and repairing. However, previous research [4–8] has shown that waterglass-activated slag mortars and concretes are subject to substantial autogenous and drying shrinkage, this being one of the main drawbacks to the definitive use of AAS as an alternative to traditional Portland cement binders. Nevertheless, the origin of this shrinkage has not yet been fully explained.

Some authors [9,10] suggest that the characteristics of the hydrated calcium silicate gel and pore size distribution, have a direct effect on drying shrinkage. According to Kutti [11] two main hydration products are formed as a result of alkali activation of slag, a C–S–H gel similar to the gel formed in Portland cement pastes, although with a lower Ca/Si ratio, and a Si-rich gel with properties similar to silica gel. This latter product contains a higher uncombined water content that is eliminated during the drying process, causing substantial shrinkage and therefore microcracking.

Other researchers [11,12] have concluded that alkali-activated slag concretes and mortars have a lower total porosity and a larger refined pore structure than the respective Portland cements. According to the results reported by Shi [12], Portland cement

* Corresponding author.
E-mail addresses: martapalacios@ietcc.csic.es (M. Palacios), puertasf@ietcc.csic.es (F. Puertas).

0008-8846/$ - see front matter © 2007 Elsevier Ltd. All rights reserved.
doi:10.1016/j.cemconres.2006.11.021

mortars exhibit a continuous pore distribution with sizes ranging from 50 to 12,000 Å, whereas alkali-activated slag mortars only have pores with diameters of under 100 and over 2000 Å. In this regard, Collins et al. [13] studied the relationship between such a pore size distribution and drying shrinkage in alkali-activated slag concretes, concluding that the higher mesopore content in waterglass-activated slag concretes (~ 74–82%) compared to Portland cement concretes entails higher capillary stress and therefore greater shrinkage during drying.

Lower shrinkage is believed to be favoured in slags with high specific surface areas, low activator solution/slag ratios, low waterglass modules, low activator concentration and high aggregate/slag ratios [14]. Very few authors, however, have studied the possible ways of reducing such shrinkage. Further to the results reported by Puertas et al. [15], the use of polypropylene fibres slightly decreases shrinkage in waterglass-activated mortars cured at 50% relative humidity (RH). Bakharev et al. [16] studied the effect of different admixtures on shrinkage in waterglass-activated slag concrete, concluding that gypsum reduces both autogenous and drying shrinkage thanks to the formation of expansive phases such as ettringite (AF_t). Shrinkage is increased, in turn by the addition of naphthalene-based organic admixtures, and lowered with lignosulphate, air-entraining and shrinkage-reducing admixtures.

The effect of shrinkage-reducing admixtures (SRA) has been amply studied in Portland cement systems [17,18], where they decrease capillary stress in pore water, which in turn reduces cement paste shrinkage.

However, the effect of SRA on the pore structure, mineralogical composition and microstructure of activated slag pastes and mortars has not been determined to date, and constitutes the object of the present study.

2. Experimental

2.1. Materials used

The chemical composition of the blast furnace slag used in this study is shown in Table 1. The slag had a specific surface area of 325 m^2/kg and a 99% vitreous phase content.

The slag was alkali-activated with a waterglass ($Na_2O{\cdot}nSiO_2{\cdot}mH_2O$+NaOH) solution having a Na_2O/SiO_2 ratio of 1.0–1.2 and a Na_2O concentration of 4% (by mass of slag). A SRA, based on polypropylenglycol, was added at dosages from 0 to 2% (by mass of slag). The admixture was mixed with the activator solution.

A cement type CEM I 42.5R was used as a reference material. The chemical composition is shown in Table 1 and the specific area was 360 m^2/kg.

Table 2
Solid/liquid ratio of the mortars

Mortars	*l*/*s* ratio
Slag + waterglass	0.58
Slag + waterglass + 1% SRA	0.55
Slag + waterglass + 2% SRA	0.50
Cement	0.42

2.2. Mortar preparation and testing

Alkali-activated slag (AAS) mortars, with and without SRA, and Portland cement (OPC) mortars were prepared with an aggregate/binder ratio of 2/1. Mortars were made with a siliceous (99% SiO_2, quartz) aggregate. The liquid/solid (*l*/*s*) ratios used, shown in Table 2, were determined from the results of slump tests conducted to Spanish standard UNE-80–116–86.

The mortars were tested as follows:

2.2.1. Strength

AAS mortars (4×4×16 cm) were prepared according to Spanish standard UNE-196–1. These waterglass-activated specimens were cured at 20±2 °C and 99% relative humidity (RH) for 48 h. They were subsequently removed from the moulds and cured until the day of the strength test at 99% or 50% relative humidity (RH).

The flexural and compressive strengths of the specimens were measured after 2, 7 and 28 days as specified in European standard UNE-EN 196–1-1994.

2.2.2. Shrinkage

Prismatic waterglass-activated slag and Portland cement mortar specimens measuring 2.5×2.5×28.7 cm were prepared with and without SRA. The specimens were cured as described above and placed in a humidity chamber at either 99% or 50% RH after removal from the moulds. Shrinkage was determined as specified in Spanish standard UNE 80–112–89.

2.2.3. Mercury intrusion porosimetry

At 2, 7, 28, 60 and 120 days of curing, total porosimetry and pore size distribution were determined in waterglass-activated slag mortars, with and without SRA, by a Micromeritics 9320 porosimeter. These parameters were determined on AAS mortars (4×4×16 cm) cured at 99% and 50% of relative humidity with a dimension of 4×4×16 cm.

2.3. Effect of SRA on alkaline activation of slag pastes

The slag activation process was studied by isothermal heat conduction calorimetry on waterglass-activated slag pastes

Table 1
Chemical analysis of blast furnace slag and cement

	CaO	SiO_2	Al_2O_3	MgO	Fe_2O_3	SO_3^-	S^{2-}	Na_2O	K_2O	L.O.I*	I.R**
Slag	41.37	34.95	13.11	7.12	0.69	0.04	1.92	0.27	0.23	2.02	0.11
Cement	64.41	17.91	5.17	1.30	3.85	2.64	–	0.39	0.78	0.78	0.29

* L.O.I.: loss of ignition; ** I.R.: insoluble residue.

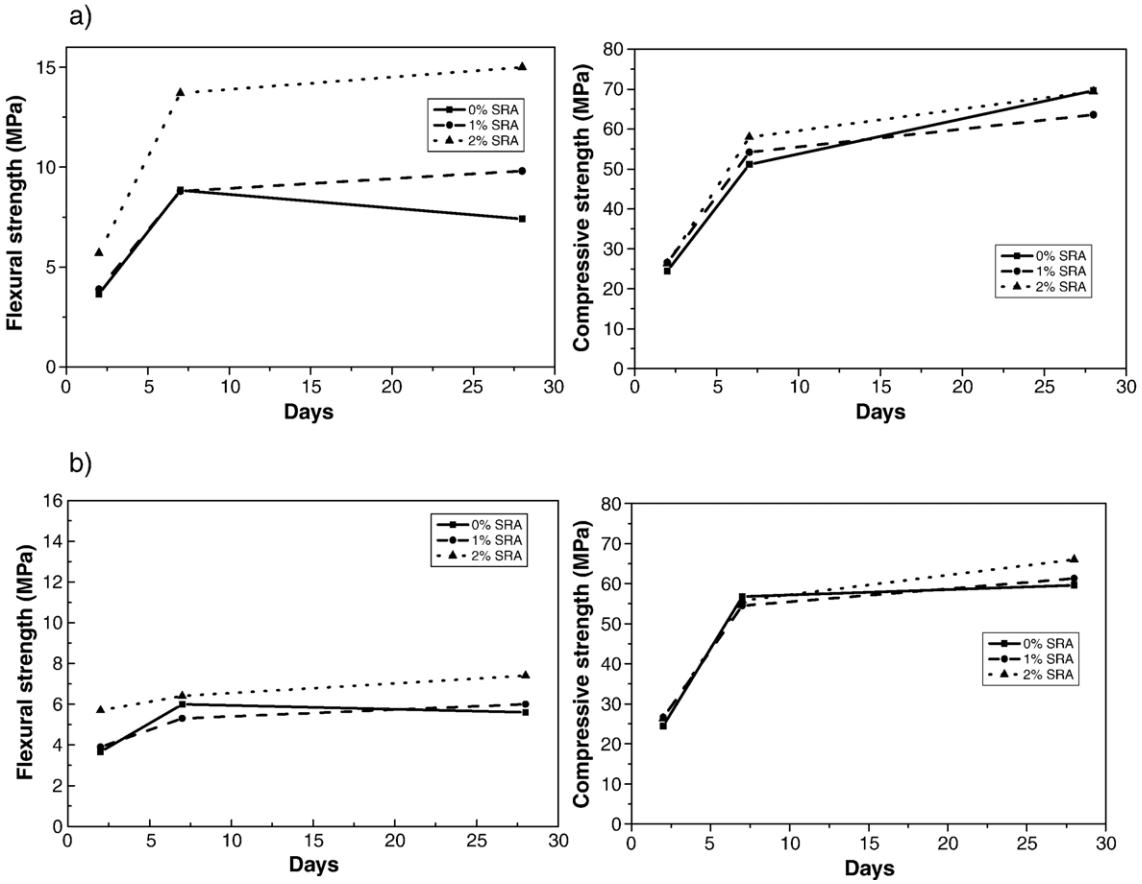

Fig. 1. Mechanical strength values for waterglass-activated slag mortars with and without SRA under different curing conditions: a) RH = 99% and b) RH = 50%.

prepared with SRA dosages from 0 to 2% (by mass of slag). The solid/liquid ratio used was 0.5.

A JAF isothermal heat conduction calorimeter was used for this test, run on specimens for 70 h at 25 °C. 20 g of blast furnace slag were mixed in a plastic bag with 10 g of alkaline solution which contains dosages of SRA from 0 to 2%. After the sample was incorporated into a steel cell of the calorimeter, it was introduced into a bath of water at 25 °C.

2.4. Paste mineralogy and microstructure

Waterglass-activated slag pastes were prepared with SRA at dosages ranging from 0 to 2% (by mass of slag) and a liquid/solid ratio of 0.5. The pastes were placed in a curing chamber at 20±2 °C and RH = 99% for 48 h. After removal from the moulds, the pastes were cured at RH = 99% or RH = 50%, for up to 7 days, after which they were immersed in acetone in order to stop the hydration of the slag and examined by:

a) Fourier transform infrared spectroscopy (FTIR) with an FTIR ATIMATTSON GENESIS instrument. KBr pellets were prepared for scanning, which was performed across a frequency range of 4000 to 400 cm^{-1}.
b) X-ray diffraction (XRD) with a Philips PW-1730 diffractometer; the 2Θ angles studied ranged from 5° to 60°.
c) ^{29}Si and ^{27}Al magic angle solid-state nuclear magnetic resonance spectroscopy (MAS NMR) with BRUKER MSL 400 equipment. The recording conditions for ^{29}Si were: resonance frequency 79.49 MHz; number of scans per sample 800; relaxation time 5 s; and sample rotation speed 4 KHz. The chemical signal obtained was measured in ppm, with trimethylsilane (TMS) as the external chemical shift reference.
The recording conditions for ^{27}Al were: resonance frequency 104.2 MHz; number of scans per sample 200; relaxation time 5 s; and sample rotation speed 12 KHz. The chemical signal obtained was measured in ppm, with aluminium trichloride as the external chemical shift reference.
d) Scanning electron microscopy (SEM) and energy dispersion X-ray spectroscopy (EDX) with A JEOL 5400 scanning electron microscope, in combination with a SYSTEM ISIS EDX OXFORD-LINK solid-state backscattered detector. Carbon coating was necessary to make the samples conductive under electronic microscope.

3. Results

3.1. Strength

The development of mechanical strength of waterglass-activated slag mortars, with and without SRA, as well as for

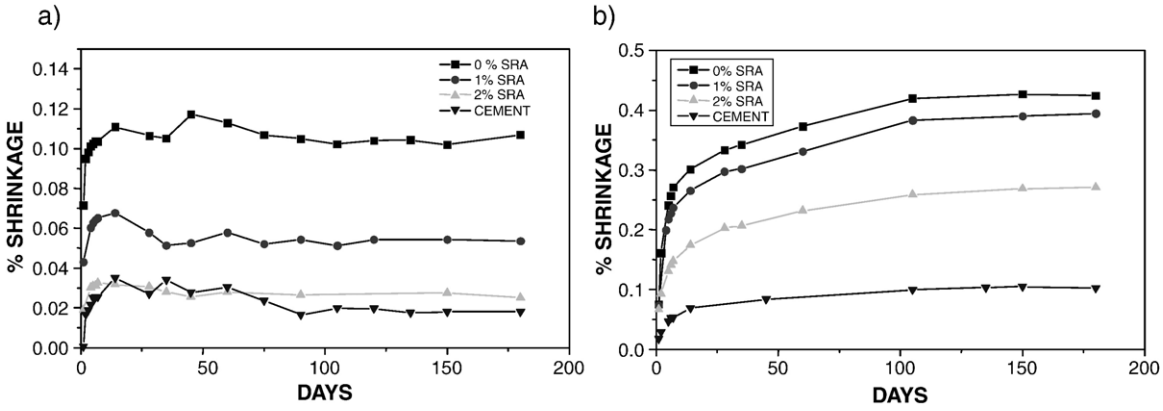

Fig. 2. Shrinkage in waterglass-activated slag mortars, with and without SRA, under different curing conditions: a) RH=99% and b) RH=50%.

Portland cement mortars, are given in Fig. 1. This Figure also shows the effect of relative humidity of curing conditions on mortar strengths.

The addition of 1% SRA did not significantly modify the flexural or compressive strength of waterglass-activated slag mortar cured at either 99% or 50% RH, although after 28 days, the flexural strength of the specimens cured at RH=99% was 25% higher than recorded for the mortars without admixture.

The addition of 2% SRA increased the flexural strength of the waterglass-AAS mortar specimens prepared under both curing conditions, although more significantly in the mortars cured at 99% RH: flexural strength was increased by ~75% at 7 days, and by more than 100% at 28 days relative to the mortars without SRA. SRA did not, however, induce any substantial change in compressive strength compared to the specimens without admixtures under either of the curing conditions.

3.2. Shrinkage

Shrinkage of Portland cement and waterglass-AAS mortars, with and without SRA, under both curing conditions (99% and 50% RH) are shown in Fig. 2.

When the waterglass-AAS mortars were cured at RH=99%, the addition of 1% SRA reduced the shrinkage (which in this case may be regarded to be autogenous shrinkage) by up to 50%; the addition of 2% SRA lowered shrinkage by up to 85%, bringing it down to values similar to those found for Portland cement mortars. When the specimens were cured at a relative humidity of 50%, the addition of 1% SRA reduced shrinkage by only 7%, while the 2% SRA dosage of the same admixture generated a 50% decline. In this case, despite the substantial drop in the shrinkage rate, it was still twice as large as in Portland cement mortars.

3.3. Total porosity and pore size distribution

Table 3 shows the total porosity and average pore diameter of the different waterglass-AAS mortars – i.e., with and without SRA and cured at 99% and 50% relative humidity – while Fig. 3 gives their pore size distribution.

It may be deduced from the data in Table 3 that the total porosity values and their evolution during curing is very similar for all the mortars, with barely any variation detected between mortars prepared with different admixture dosages or under different curing conditions.

Variations were, however, observed in the average pore diameter in waterglass-activated slag mortars, depending on curing conditions and the presence/absence and dosages of the SRA admixture. After 28 days, the average pore diameter was found to be smaller in specimens cured at RH=99% than at RH=50%. Furthermore, the addition of SRA reduced the average pore diameter in the mortars studied after 2 days of curing; this

Table 3
Total porosity and average pore diameter in the AAS mortars

Relativ humidity	Mortar	Curing days	Total porosity (%)	Average pore diameter (μm)
99%	Slag+waterglass	2 days	13.09	0.0216
		7 days	10.64	0.0171
		28 days	13.23	0.0163
		60 days	9.64	0.0143
		120 days	9.18	0.0127
	Slag+waterglass+1% SRA	2 days	12.82	0.0180
		7 days	9.90	0.0164
		28 days	12.07	0.0145
		60 days	10.22	0.0140
		120 days	8.82	0.0110
	Slag+waterglass+2% SRA	2 days	12.70	0.0168
		7 days	10.60	0.0164
		28 days	10.89	0.0146
		60 days	9.95	0.0156
		120 days	9.12	0.0163
50%	Slag+waterglass	2 days	13.09	0.0216
		7 days	10.63	0.0164
		28 days	13.55	0.0155
		60 days	13.07	0.0229
		120 days	9.73	0.0145
	Slag+waterglass+1% SRA	2 days	12.82	0.0180
		7 days	10.78	0.0157
		28 days	12.47	0.0138
		60 days	10.75	0.0167
		120 days	8.94	0.0160
	Slag+waterglass+2% SRA	2 days	12.70	0.0168
		7 days	9.78	0.0161
		28 days	11.61	0.0160
		60 days	10.91	0.0169
		120 days	10.30	0.0218

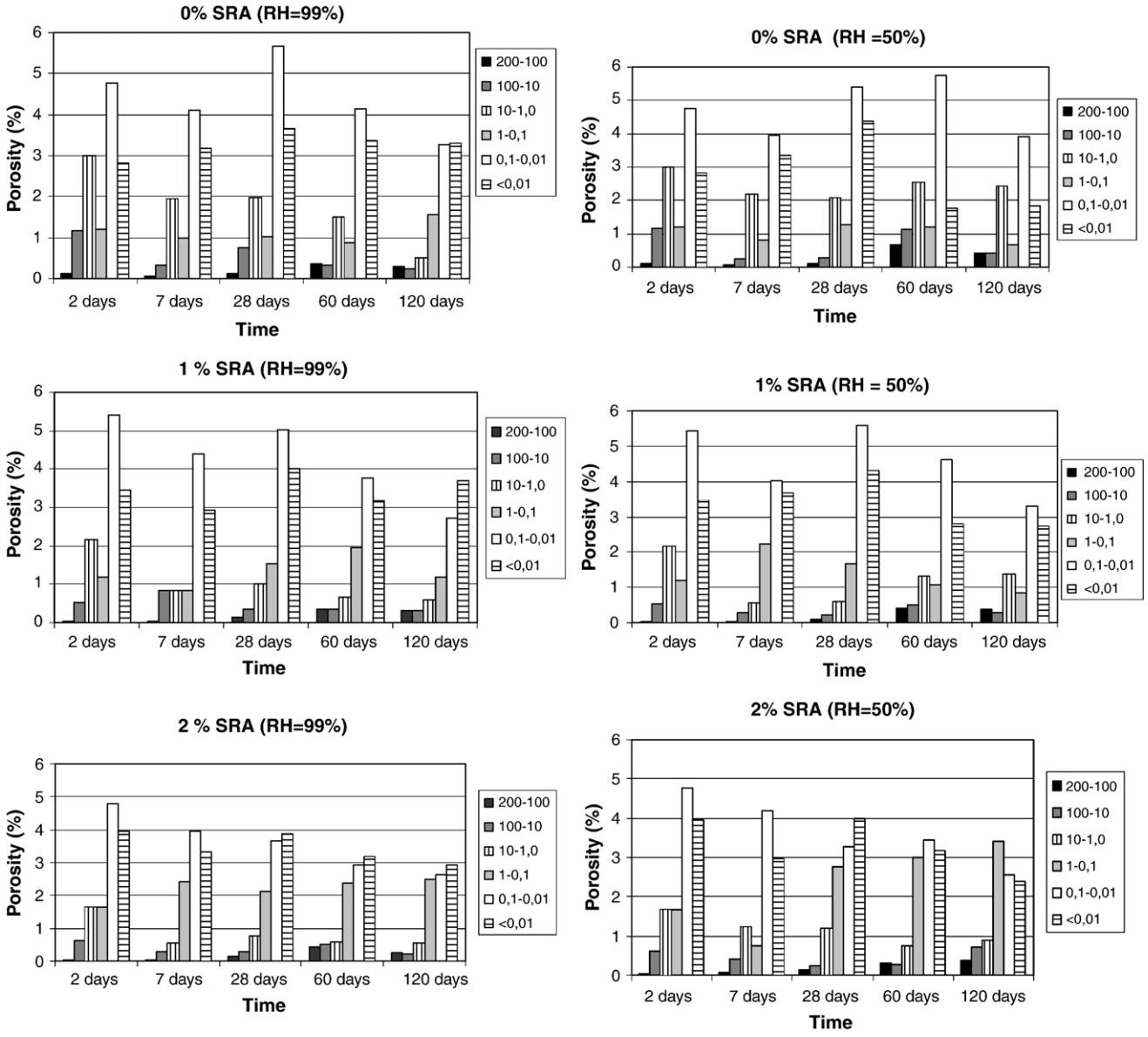

Fig. 3. Pore size distribution (in μm units) in waterglass-activated slag mortars, with and without SRA, under different curing conditions: RH = 99% and RH = 50%.

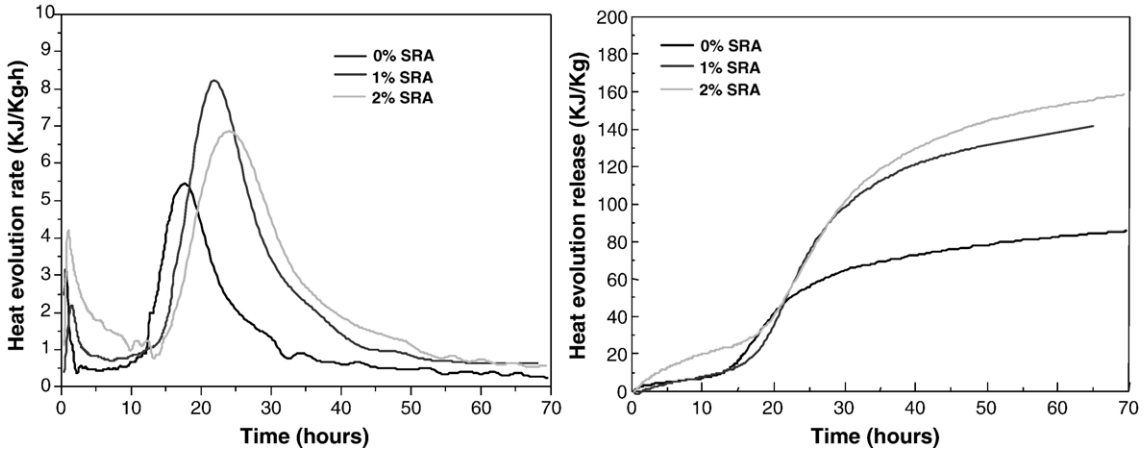

Fig. 4. Heat evolution rate and total heat release curves for alkali-activated slag pastes.

Table 4
Calorimetric data for waterglass-activated slag pastes

% SRA	Aceleration signal			Total heat (KJ/Kg)
	Time (h)	Maximum rate (KJ/Kg h)	Heat released (KJ/Kg)	
0	17.7	5.7	78.2	85.3
1	21.5	8.8	136.8	145.0
2	24.4	6.8	137.2	157.5

reduction decreased over time in mortars with 1% admixture and remained practically unchanged with 2% dosages of SRA.

Relative humidity, in turn, had no significant early age effect on pore size distribution in the mortars studied; after 28 days, however, the mortars cured at 99% relative humidity showed higher percentages of pores with diameters under 0.01 μm than the specimens cured at 50% RH.

The addition of 1% and 2% SRA in alkali-activated slag mortars cured at 99% RH for 2 days increased the percentage of pores with diameters of under 0.01 μm. After 28 days at both RH = 99% and RH = 50%, the mortars containing 1% SRA had a higher percentage of pores with sizes ranging from 1.0 to 0.1 μm than mortars without admixture. The addition of 2% SRA reduced the percentage of pores with diameters ranging from 0.1 to 0.01 μm and increased the proportion with diameters of from 1.0 to 0.1 μm, at all the ages studied.

3.4. Effect of SRA on paste alkali activation

Fig. 4 shows the heat evolution rate and total heat released in the slag activation reaction.

The different peaks visible on the heat evolution rate graph are associated with the various stages of the slag activation process [19,20] A first peak, associated with the partial dissolution of the slag in the highly alkaline medium, was not recorded due as this occurs very rapidly, i.e. before the start of measurements. The first recorded peak (appearing within the first 2 h) corresponds to the pre-induction period, when the silicate ions in the waterglass solution react with the Ca^{2+} ions in the slag to form an initial C–S–H gel. The formation of this C–S–H gel around the anhydrous slag particles inhibits their activation during the induction period. A third, very intense heat evolution rate peak was recorded as the reaction products precipitated during the acceleration period. Finally, the product precipitation rate declined during the deceleration period.

The results shown in Table 4 indicate that the addition of SRA retarded slag activation, with the third peak appearing at 17.7, 21.5 and 24.4 h when SRA dosage was 0, 1 and 2%, respectively. The addition of SRA also lengthened the pre-induction period by up to two hours. Table 4 shows that the presence of the SRA increased the maximum heat evolution rate, with values of 5.7, 8.8 and 6.8 KJ/Kg h when 0, 1 and 2% and SRA was added, respectively. Finally, in the presence of the admixture, mass precipitation of reaction product continued over a longer period of time and the total heat which was released in the process was greater.

3.5. Paste mineralogy and microstructure

3.5.1. Fourier transform infrared spectroscopy

Fig. 5 shows the infrared spectra for the slag pastes prepared with different dosages of SRA and cured at different relative humidities (99% and 50%).

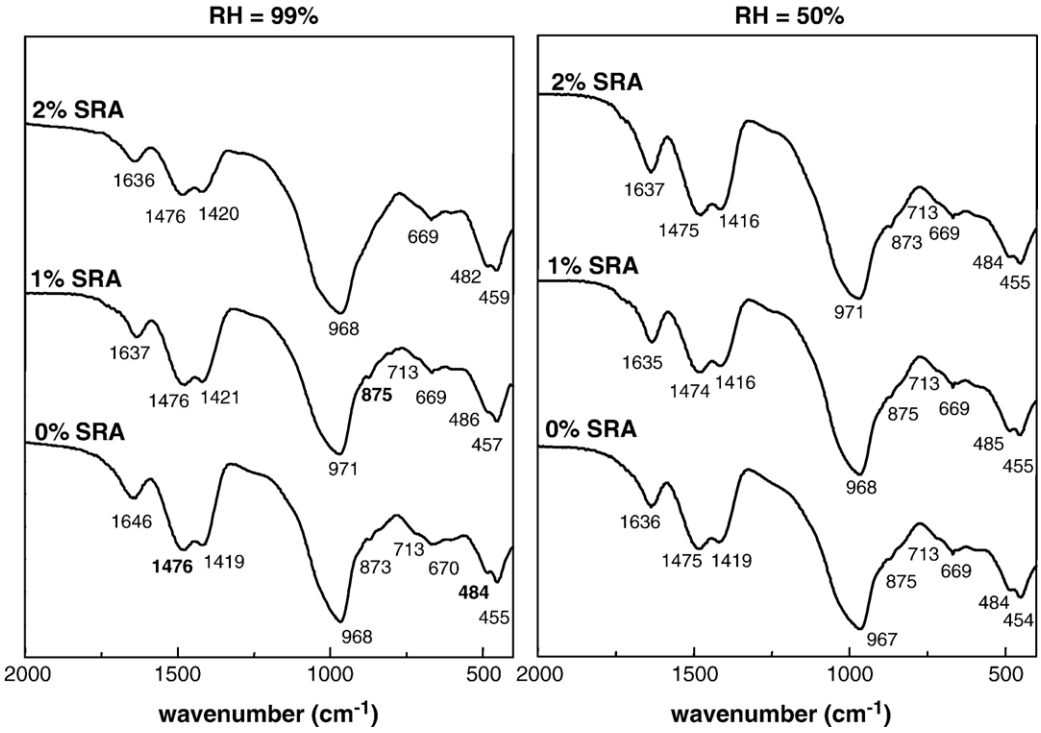

Fig. 5. FTIR spectra for waterglass-activated slag pastes cured at 99% and 50% relative humidity.

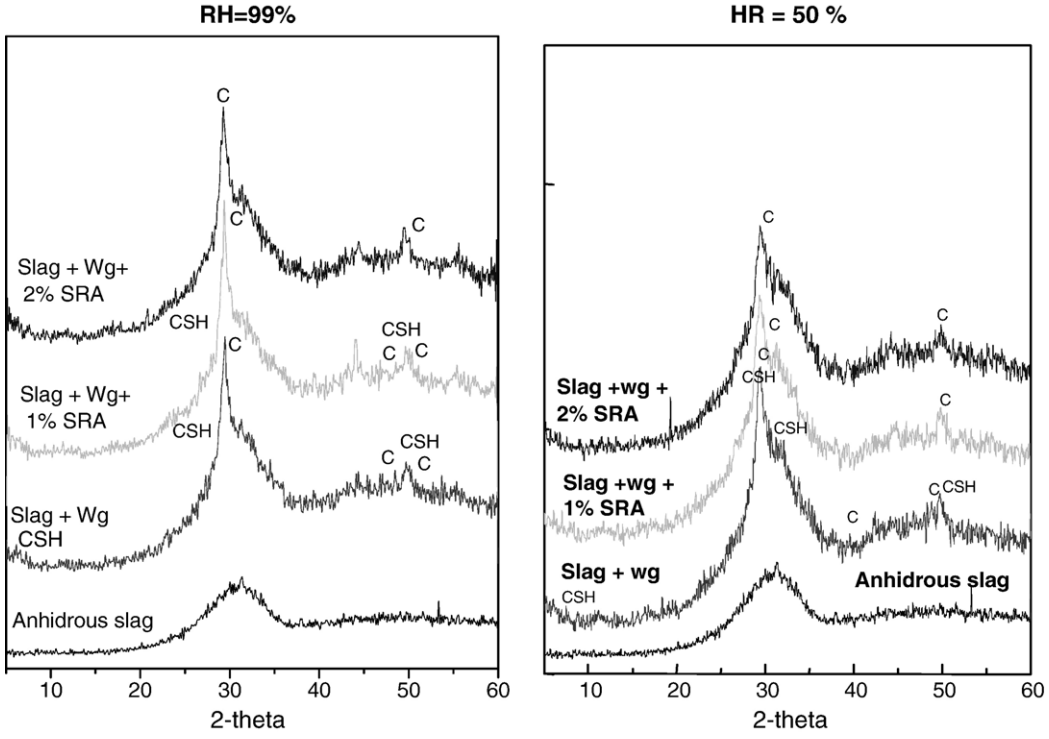

Fig. 6. Diffractograms of waterglass-activated slag pastes cured at 99% and 50% relative humidity. CSH=CSH gel; C=$CaCO_3$.

The infrared spectra of all the pastes studied had vibration bands at around 967–971 cm^{-1}, associated with the Si–O (v_3 (Si–O)) stretching vibration in the SiO_4 tetrahedra comprising the C–S–H gel. The two bands appearing between 454 and 486 cm^{-1} were attributed to the O–Si–O (v_4 (O–Si–O)) deformation vibration, while the band observed at 669 cm^{-1} was attributed to the Al–O stretching vibration in AlO_4 groups.

The aragonite and calcite v_3 $[CO_3]^{2-}$ vibration bands appeared at 1475 and 1420 cm^{-1}, respectively, while the v_2 $[CO_3]^{2-}$ and v_4 $[CO_3]^{2-}$ vibration bands for the carbonates were observed at 875 and 713 cm^{-1}.

Neither the presence of the SRA nor the differences in relative humidity induced changes in the infrared spectra of the pastes studied.

3.5.2. X-ray diffraction (XRD)

Fig. 6 shows the XRD patterns for the pastes with and without admixture and cured at relative humidities of 99% and 50%.

Although the semi-crystallinity of the C–S–H gel (2Θ=7.07, 29.09, 31.96 and 49.83) renders its XRD identification particularly difficult, the presence of the calcite formed as a result of the interaction between atmospheric CO_2 and the dissolved Ca^{2+} from the slag is readily identifiable.

Neither the presence of the admixture nor the differences in relative humidity induced changes in the mineral composition of the pastes characterized with XRD techniques.

3.5.3. Nuclear magnetic resonance spectroscopy (MAS NMR)

Fig. 7 shows the ^{29}Si and ^{27}Al MAS NMR spectra of the alkali-activated slag pastes with and without shrinkage-reducing admixture and cured at different relative humidities (99% and 50%). The results of deconvolution of these ^{29}Si and ^{27}Al MAS NMR spectra are given in Tables 5 and 6. Table 7 lists the data on degree of reaction, length of chain and Al/Si ratio calculated according to the equations proposed by Richardson [21].

The ^{29}Si MAS NMR spectra of the 7-day waterglass-activated slag pastes have signals centred at around −68 ppm and −73 ppm, attributed to Si Q^0 and Q^1 of the unreacted anhydrous slag, and three further signals at −78 ppm, −81.5 ppm and −85 ppm, attributed to Si Q^1, Q^2 and Q^2(1Al), respectively [22].

Pastes cured at 50% RH have a higher percentage of Si Q^0+Q^1 units from the unreacted anhydrous slag and slight short chains in the C–S–H gel (see Table 6). This Table also shows that at 50% RH, the Al/Si and the $\Sigma Q^2/Q^1$ ratios in the C–S–H gel formed were likewise lower.

According to Table 5, when the pastes were cured at RH=99%, the addition of 1% of SRA did not significantly modify the percentages of tetrahedrally co-ordinated Si units; the addition of a 2% dosage, however, reduced the percentage of Si Q^2(1Al) units.

The ^{29}Si MAS NMR spectra of the waterglass-activated slag pastes cured at RH=50% show that the presence of the admixture generated an increase in the amount of unreacted anhydrous slag and therefore reduced the degree of reaction. As when RH=99%, at RH=50%, the addition of 2% of the SRA admixture reduced the Al content in the C–S–H gel, as may be deduced from the decrease in the Al/Si ratio and the increase in the Q^2/Q^2(1Al) ratio.

Three signals were observed on the ^{27}Al MAS NMR spectra for waterglass-activated slag: ~63.0 ppm, ~35.0 ppm and

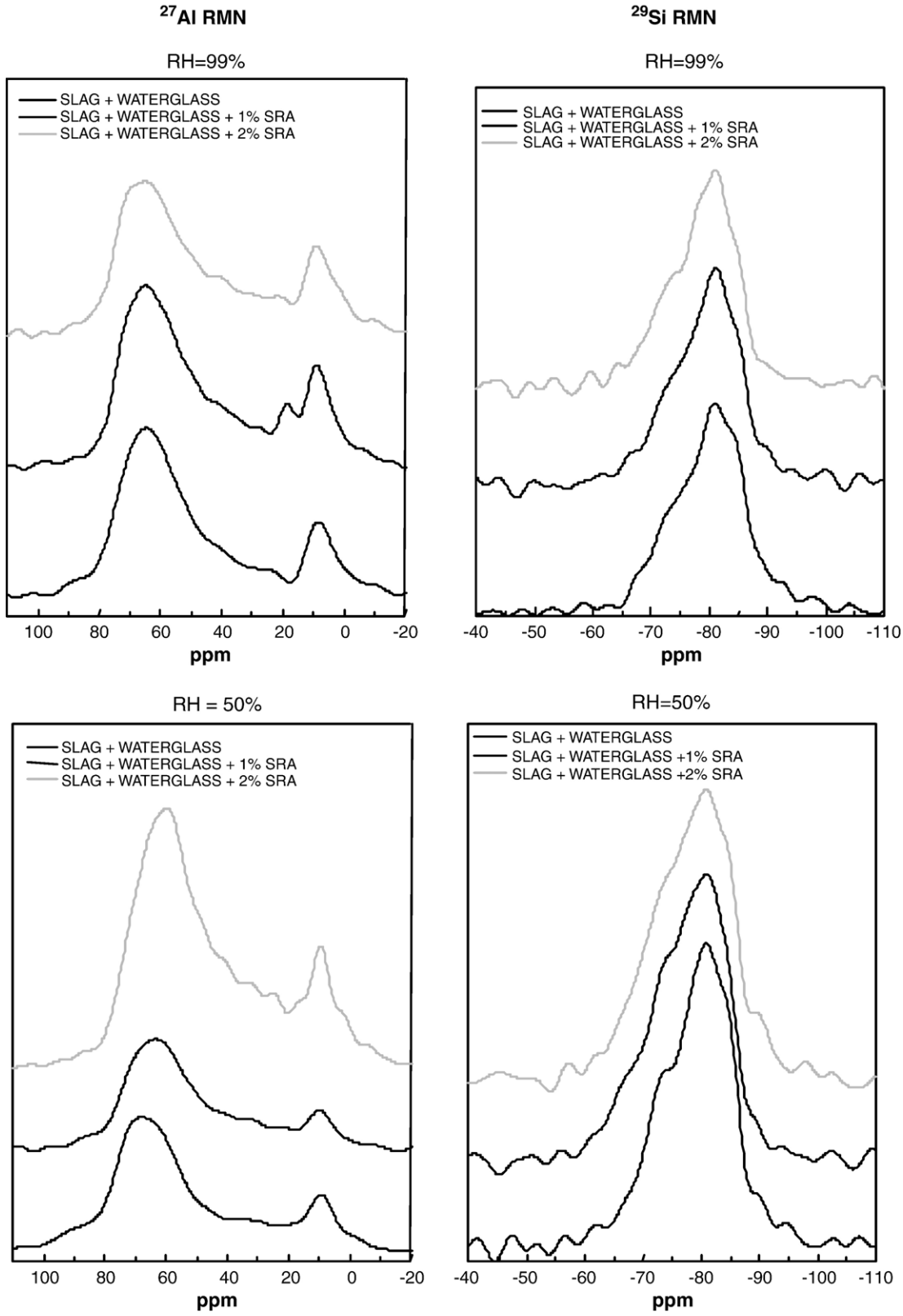

Fig. 7. ^{29}Si and ^{27}Al MAS NMR spectra for waterglass-activated slag pastes.

~8.0 ppm (see Fig. 7), corresponding to tetrahedral, pentahedral and octahedral Al units, respectively [22]. The relative humidity of the curing condition had no effect on the percentages of the various Al units, although at both RH=99% and RH=50% the proportion of tetrahedral Al units declined in the presence of the SRA admixture (Table 6).

Table 5
Results obtained after deconvolution of the ^{27}Si MAS NMR spectra of waterglass-activated slag pastes, with and without shrinkage reduction admixture

RH	% Admixture	Q^0	Q^1(Slag)	Q^1 (End of chain)	Q^2(1Al)	Q^2 (0Al)
99%	0%	−68.0 ppm	−73.5 ppm	−77.8 ppm	−81.8 ppm	−85.3 ppm
		I=7.42%	22.70%	20.31%	31.69%	17.88%
	1%	−67.0 ppm	−73.0 ppm	−77.7 ppm	−81.4 ppm	−85.1 ppm
		I=6.86%	I=23.07%	I=20.85%	I=31.68%	I=17.53%
	2%	−68.0 ppm	−73.5 ppm	−77.9 ppm	−81.2 ppm	−85.00 ppm
		I=7.56%	I=24.74%	I=18.65%	I=29.30%	I=19.76%
50%	0%	−66.7 ppm	−73.3 ppm	−78.5 ppm	−81.9 ppm	−85.0 ppm
		I=6.71%	26.39%	23.35%	26.39%	17.15%
	1%	−66.7 ppm	−73.5 ppm	−78.1 ppm	−81.5 ppm	−84.9 ppm
		I=12.08%	I=28.29%	I=19.79%	I=23.77%	I=16.07%
	2%	−67.1 ppm	−73.4 ppm	−78.25 ppm	−81.5 ppm	−84.75 ppm
		I=10.34%	I=28.91%	I=20.24%	I=21.69%	I=18.81%

3.5.4. Scanning electron microscopy (SEM)

A scanning electron microscopic study was conducted to the microstructure of the 7-day waterglass-activated slag pastes, cured at 99% and 50% relative humidity.

In all the cases studied, the micrographs (Fig. 8) show very compact pastes with a chemical composition based on Ca, Si and Al and small percentages of Na, Mg, S and Fe. In the absence of the SRA admixture, the pastes cured at both relative humidities exhibited intense cracking as a result of the substantial shrinkage taking place. The addition of the SRA reduced both the number and width of these cracks.

4. Discussion

The addition of SRA reduced shrinkage in alkali-activated slag mortars by up to 85% or 50%, when cured at 99% or 50% relative humidity, respectively. This beneficial effect of the admixture on shrinkage was visible with SEM/EDX techniques (see Fig. 8). The micrographs of the waterglass-activated slag pastes, cured under both relative humidity conditions, show that the presence of SRA reduces the number and width of the shrinkage-generated microcracks. The higher the dosage of admixture, the more effective was shrinkage decrease.

Table 6
Results obtained after deconvolution of the ^{27}Al MAS NMR spectra of waterglass-activated slag pastes, with and without shrinkage reduction admixture

RH	% admixture	Al_t	Al_p	Al_o
99%	0%	63.75 ppm	35.50 ppm	7.70 ppm
		I=71.88%	11.84%	16.28%
	1%	63.70 ppm	35.00 ppm	8.96 ppm
		I=60.39%	17.77%	21.84%
	2%	64.25 ppm	35.01 ppm	7.86 ppm
		I=57.36%	21.41%	21.22%
50%	0%	63.63 ppm	32.65 ppm	8.64 ppm
		I=69.92%	15.16%	14.92%
	1%	66.63 ppm	33.72 ppm	9.63 ppm
		I=64.21%	21.31%	14.47%
	2%	60.76 ppm	33.31 ppm	9.21 ppm
		I=62.19%	22.39%	15.42%

Several authors [10,11,14] explain the severe shrinkage in alkali-activated slag systems in terms of their porous structure and the microstructure of the C–S–H gel formed.

The addition of SRA did not significantly modify total porosity in waterglass-activated slag mortars, although it did reduce the average pore diameter in mortars cured for 2 days.

At a relative humidity of 99%, alkali-activated slag mortars undergo autogenous shrinkage, as a result of two developments, chemical shrinkage and self-drying shrinkage. The former can be attributed to the larger space occupied by the hydration products than the initial constituents. Moreover, the hydration of anhydrous particles entails a reduction in the amount of water in the capillary pores; the reduction in the relative humidity in the pore system causes a water-air meniscus. The resulting increase in the stress on the porous structure in turn leads to self-drying shrinkage [23]. In this regard, the extensive autogenous shrinkage in waterglass-activated slag mortars (Fig. 2) can be explained by their high percentage of pores with a diameter lower than 0.1 μm (Table 3). The water meniscus formed in the capillary pores of the mortar subjects the pore walls to considerable stress that translates into substantial shrinkage. The addition of the shrinkage-reducing admixture reduces such autogenous shrinkage by up to 85%.

This beneficial effect of the SRA is due primarily to three developments: firstly, the reduction in the liquid/solid ratio; secondly, the decrease in the surface tension of the water in the porous system and the concomitantly smaller internal stress when the water evaporates [24]; thirdly, and most importantly, the redistribution of the porous structure, because the admixture increases the percentage of pores with diameters ranging from

Table 7
Parameters obtained with ^{27}Si MAS NMR (Fig. 7)

RH	Admixture	$\alpha=(1-(Q^0+Q_{slag}))*100$	$\Sigma Q^2/Q_{total}$	Q^2 (0Al)/Q^2(1Al)	$\Sigma Q^2/Q^1$	CL	Al/Si
99%	0%	69.88	0.71	0.56	2.44	8.44	0.23
	1%	70.07	0.70	0.55	2.36	8.28	0.23
	2%	67.7	0.72	0.67	2.63	8.83	0.22
50%	0%	66.9	0.65	0.65	1.86	6.86	0.20
	1%	59.63	0.67	0.68	2.01	7.22	0.20
	2%	60.75	0.67	0.87	2.00	7.07	0.18

1.0 to 0.1 μm, which exhibit a capillary stress much lower than the smaller pores that prevail in mortars without admixture, subjected to longer curing periods. This redistribution of the pores is due to the decrease of the capillary stress of the water that SRA induces during the mixing process.

When the relative humidity of the curing environment was reduced, in addition to autogenous shrinkage, waterglass-activated slag mortars suffers from drying shrinkage caused by the evaporation of the water in the capillary pores and the gel [25]. At RH = 50%, nearly all the water in the larger pores but only part of the capillary pore water (diameter lower than 0.05 μm) evaporates. Substantial stress is transferred from the aqueous phase to the pore walls in these capillary pores and may produce their collapse and the concomitant formation of microcracks [24] as shown in the micrographs. In this study, the capillary stress for mortars cured at RH = 50% was much higher than that described for mortars cured at RH = 99%, where the pore water loss was significantly lower. The addition of 2% SRA, like curing at RH = 99%, reduced drying shrinkage and for the same reason: i.e., it induces a decrease in the demand for liquid in the mortar mix while reducing the surface tension of the pore water. The latter facilitates the elimination of the pore water, in turn reducing the capillary stress that causes greater shrinkage. In this case also, the percentage of pores with diameters ranging from 1.0 and 0.1 μm, in which capillary stress is lower, was higher than in mortars without admixture.

The MAS NMR results on the microstructure of the C–S–H gel in alkali-activated slag mortars show that in the absence of

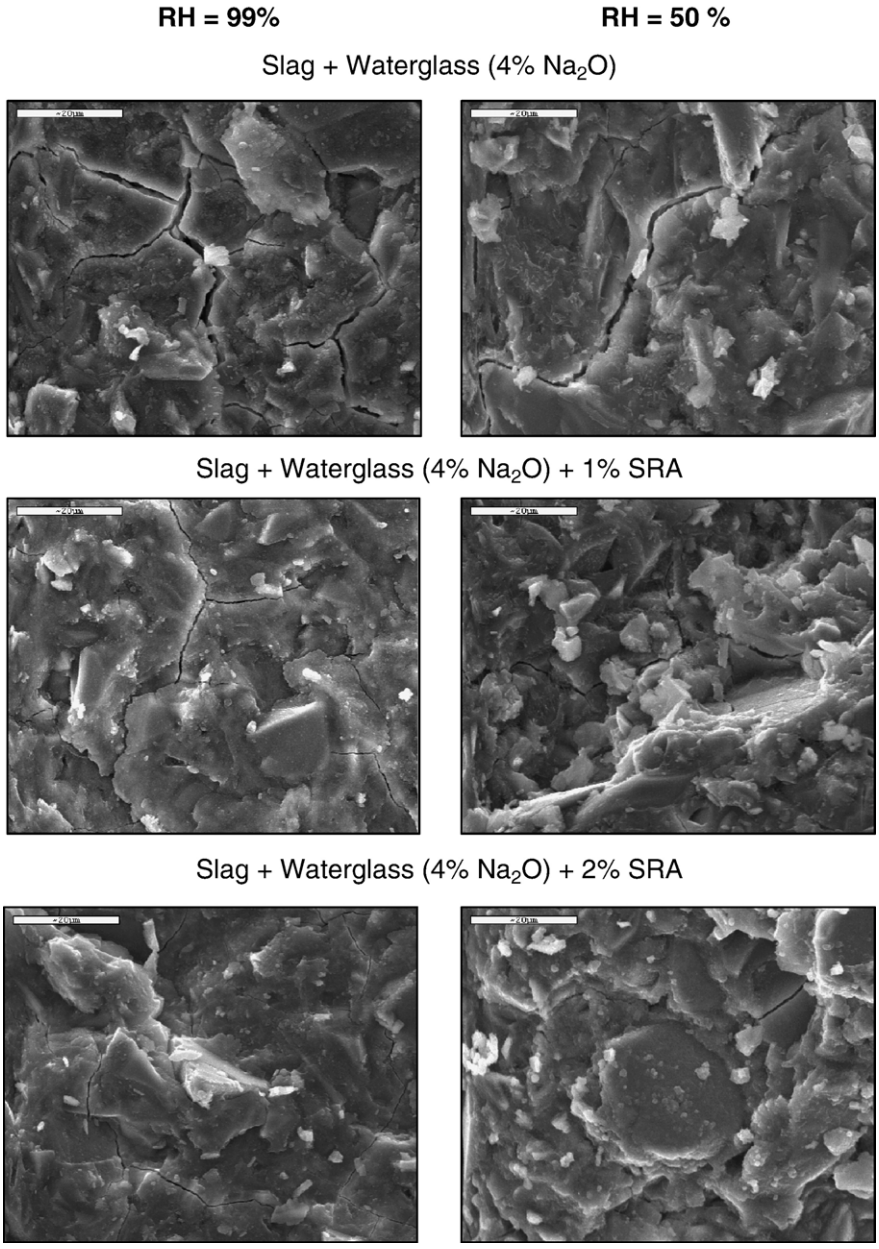

Fig. 8. Waterglass-activated slag paste SEM images, in the presence and absence of a shrinkage-reducing admixture, cured at 99% and 50% relative humidity.

SRA, reducing the relative humidity of the curing condition from 99% to 50% lowers the degree of reaction and consequently the $\Sigma Q^2/Q^1$ ratio, as well as the average length of the silicate chains comprising the C–S–H gel. Furthermore, the decrease in environmental relative humidity also prompted greater Si replacement by Al in the bridging tetrahedra in the C–S–H gel [26,27]. Under both curing conditions, however, the shrinkage-reducing admixture was observed to produce a slight increase in the proportion of Si Q^2 (0Al) units and a concomitant decrease in the percentage of Si Q^2(1Al) units in the C–S–H. The decline in the Al replacing the Si in the C–S–H gel structure was also observed in the ^{27}Al MAS NMR spectra (see Fig. 6). Finally, the drop in the proportion of Al_T in the pastes with SRA compared to those without SRA can likewise be deduced from the deconvolution of these spectra (see Table 7). Further studies are required in order to explain this decline of Al_T in the AAS pastes which contain SRA.

Conduction heat calorimetry, in turn, showed that the SRA retarded the alkali activation of slag, more intensely at the higher dosage of admixture. This delay may be the result of the decrease of the surface tension of the pore water that the presence of the admixture induces, as well as, the slight plasticizer properties that SRA shows, according to the reduction of the *l*/*s* ratio, retarding the interaction between the slag particles and alkaline activator solution. Although delayed, the precipitation of reaction products (mainly, C–S–H gel) was nevertheless more intense, that is, occurred at a higher maximum rate and released greater amounts of heat, up to twice as much as in cements with no SRA. The results obtained from running MAS NMR on alkali-activated slag pastes cured for 7 days indicate that the addition of the SRA affected the degree of reaction differently depending on the curing conditions. Slag degree of reaction was barely affected in mortars cured at 99% RH (see Table 7), whereas when they were cured at 50% RH, the presence of SRA reduced slightly the degree of reaction by 7% which could be not agree with the results obtained by calorimetry. However, it should have in account, the different age of curing of the AAS pastes in both techniques, 70 h and 7 days in samples studied by calorimetry and MAS NMR, respectively, and the different conditions of preparation of the samples in both cases.

Therefore, according to these findings, SRA reduces autogenous and drying shrinkage in waterglass-activated slag mortars, modifying the pore structure and decreasing slightly the percentage of Al in the C–S–H gel formed.

Despite the initial delay induced by SRA in the slag activation process, FTIR and XRD spectra (Figs. 4 and 5) show that after 7 days the presence of SRA had no significant effect on the mineralogical composition of the pastes cured at either RH = 99% or RH = 50%.

Finally, flexural and compressive strength rise slightly in waterglass-activated slag mortars cured at both 99% and 50% relative humidity when were prepared with SRA. This rise was due to the fact that certain fluidifying properties of the admixture prompted a reduction in the liquid/solid ratio used to prepare the mortars, by 5% at an admixture dosage of 1% and by 14% when a 2% dosage was used. This reduction of the *l*/*s* ratio induced by SRA induces, conducts to a decrease of average pore diameter, and consequently to the increase of the mechanical strength observed.

5. Conclusions

1. The shrinkage-reducing admixture based on polypropylenglycol reduces autogenous shrinkage by 85% and drying shrinkage by 50% in waterglass-activated slag mortars.
2. The beneficial effect of SRA on shrinkage is due primarily to the decline in the surface tension of the pore water and the change induced in the pore structure by the admixture. Under both curing conditions, i.e. at 99% and 50% relative humidity, the presence of the admixture increases the percentage of pores with diameters in the 1.0 to 0.1 μm range, where capillary stress is much lower than in the smaller capillaries prevailing in mortars without admixture subjected to longer curing periods.
3. ^{29}Si and ^{27}Al MAS NMR spectra show that under both curing conditions, the presence of the SRA is responsible for a slight increase in the proportion of Si Q^2 units in the C–S–H gel, and reduces the percentage of Al units replacing the Si in the gel structure.
4. The SRA admixture retards the alkali activation of slag, with longer delays at higher dosages of admixture. While delayed, the precipitation of reaction products (C–S–H gel) is nonetheless more intense: in other words, the maximum rate is higher and the heat release greater.
   The effect of SRA on the degree of reaction in 7-day slag depends on curing conditions. In mortars cured at 99% RH, the degree of reaction is barely affected, while in mortars cured at 50% relative humidity this parameter slides by 7% in the presence of the admixture.
5. The addition of SRA does not modify the mineralogical composition of the pastes cured under either of the curing conditions (RH = 99% and 50%).

Acknowledgements

Funding for project MAT 2001–1490 was provided by the Spanish Ministry of Science and Technology (MCyT). The authors wish to thank A. Gil, J. L. García, I. Sobrados, J. L. Llueca and J. L. Pita for their support in the tests conducted for this study.

References

[1] A. Fernández-Jiménez, F. Puertas, J.G. Palomo, Alkali-activated slag mortars: mechanical strength behaviour, Cem. Concr. Res. 29 (3) (1999) 593–604.
[2] F. Puertas, R. de Gutierrez, A. Fernández-Jiménez, S. Delvasto, J. Maldonado, Alkaline cement mortars. Chemical resistance to sulfate and seawater attack. Mater. Constr. 52 (267) (2002) 55–71.
[3] T. Bakharev, J.G. Sanjayan, Y.-B. Cheng, Resistance of alkali-activated slag concrete to acid attack, Cem. Concr. Res. 33 (2003) 1607–1611.
[4] E. Douglas, A. Bilodeau, V.M. Malhotra, Properties and durability of alkali-activated slag concrete, ACI Mater. J. 89 (5) (1992) 509–516.
[5] M.A. Cincotto, A.A. Melo, W.L. Repette, Effect of different activators type and dosages and relation to autogenous shrinkage of activated blast furnace

slag cement, in: G. Grieve, G. Owens (Eds.), Proceedings of the 11th International Congress on the Chemistry of Cement, Durban, vol. 4, 2003, pp. 1878–1888.
[6] F. Collins, J.G. Sanjayan, Strength and shrinkage properties of alkali-activated slag concrete containing porous coarse agrégate, Cem. Concr. Res. 29 (1999) 607–610.
[7] T. Bakharev, J.G. Sanjayan, Y.-B. Cheng, Alkali activation of Australian slag cements, Cem. Concr. Res. 29 (1999) 113–120.
[8] F. Collins, J.G. Sanjayan, Workability and mechanical properties of alkali-activated slag concrete, Cem. Concr. Res. 29 (1999) 455–458.
[9] F.H. Wittmann, Creep and shrinkage mechanisms, in: Z.P. Bazant, F.H. Witmann (Eds.), Creep and Shrinkage in Concrete Structures, Wiley, Chichester, 1982, pp. 129–161.
[10] J.F. Young, Physical mechanisms and their mathematical descriptions, in: Z.P. Bazant (Ed.), Mathematical Modelling of Creep and Shrinkage of Concrete, Wiley, Chichester, 1988, pp. 63–98.
[11] T. Kutti, Hydration products of alkali-activated slag, Proc. Int. Congr. On the Chemistry of Cement, New Delhi, vol. 4, 1992, pp. 468–474.
[12] C. Shi, Strength, pore structure and permeability of alkali-activated slag mortars, Cem. Concr. Res. 26 (12) (1996) 1789–1799.
[13] T. Häkkinen, The influence of slag content on the microstructure, permeability and mechanical properties of concrete. Part. 1, Cem. Concr. Res. 23 (1993) 407–421.
[14] F. Collins, J.G. Sanjayan, Effect of pore size distribution on drying shrinking of alkali-activated slag concrete, Cem. Concr. Res. 30 (2000) 1404–1406.
[15] F. Puertas, T. Amat, T. Vázquez, Behaviour of alkaline cement mortars reinforced with acrylic and polypropylene fibers, Mater. Constr. 50 (259) (2000) 69–84.
[16] T. Bakharev, J.G. Sanjayan, Y.-B. Chen, Effect of admixtures on properties of alkali-activated slag concrete, Cem. Concr. Res. 30 (2000) 1367–1374.
[17] N.S. Berke, M.P. Dallaire, M.C. Hicks, A. Kerkar, New Developments in Shrinkage-Reducing Admixtures. CANMET/ACI 5th International Conference on Superplasticizers and Other Chemical Admixtures in Concrete. Supplementary Papers. Ed. Malhotra. (1997) 971–998.
[18] J. Mora, A. Aguado, R. Gettu, The influence of shrinkage-reducing admixtures on plastic shrinkage, Mater. Constr. 53 (271–272) (2003) 71–80.
[19] A. Fernández-Jiménez, F. Puertas, A. Arteaga, Determination of kinetic equations of alkaline activation of blast furnace slag by means of calorimetric data, J. Therm. Anal. 52 (1998) 945–955.
[20] A. Fernández-Jiménez, F. Puertas, Effect of activator mix on the hydration and strength behaviour of alkali-activated slag cements, Adv. Cem. Res. 15 (3) (2003) 129–136.
[21] I.G. Richardson, The nature of C–S–H in hardened cements, Cem. Concr. Res. 29 (1999) 1131–1147.
[22] R.J. Kirkpatrick, Xian-Dong Cong, An introduction to ^{27}Al and ^{29}Si NMR spectroscopy of cements and concretes, in: P. Colombet, A. Grimmer (Eds.), Application of NMR Spectroscopy to Cement Science, 1994, pp. 55–76.
[23] Zhengwu Jiang, Zhenping Sun, Peiming Wang, Autogenous relative humidity change an autogenous shrinkage of high-performance cement pastes, Cem. Concr. Res. 35 (2005) 1539–1545.
[24] K.J. Folliard, N.S. Berke, Properties of high-performance concrete containing shrinkage-reducing admixture, Cem. Concr. Res. 27 (9) (1997) 1357–1364.
[25] P. Kumar Mehta. Concrete: Structure, Properties and Materials. (1986). Ed. Prentice Hall.
[26] A. Fernández-Jiménez, F. Puertas, I. Sobrados, J. Sanz, Structure of calcium silicate hidrates formed in alkaline activated slag. Influence of the type of alkaline activator, J. Am. Ceram. Soc. 86 (3) (2003) 1389–1394.
[27] P.J. Schilling, L.G. Butler, A. Roy, H.C. Heaton, ^{29}Si and ^{27}Al MAS NMR of NaOH activated blast furnace slag, J. Am. Ceram. Soc. 77 (9) (1994) 2363–2368.